Petroleum Science 20 (2023) 1690–1706

Contents lists available at ScienceDirect

Petroleum Science

journal homepage: www.keaipublishing.com/en/journals/petroleum-science

Original Paper

Laboratory study of the factors affecting hydraulic fracturing effect for inter-salt oil shale layers, Qianjiang Depression, China

Jun Zhou [a], Guang-Ai Wu [a], Ya-Nan Geng [a], Yin-Tong Guo [b, c, *], Xin Chang [b, c], Cheng-Yong Peng [a], Chuan-Zhi Ai [a]

[a] CNOOC Research Institute Ltd., Beijing, 100028, China
[b] State Key Laboratory of Geomechanics and Geotechnical Engineering, Institute of Rock and Soil Mechanics, Chinese Academy of Sciences, Wuhan, 430071, Hubei, China
[c] University of Chinese Academy of Sciences, Beijing, 100049, China

ARTICLE INFO

Article history:
Received 13 April 2022
Received in revised form
3 January 2023
Accepted 5 January 2023
Available online 6 January 2023

Edited by Yan-Hua Sun

Keywords:
Shale oil
Salt rock
Qianjiang Depression
Hydraulic fracturing
Recrystallization

ABSTRACT

This study aims to investigate the potential factors affecting hydraulic fracturing of inter-salt oil shale reservoirs in the Qianjiang Depression, China. Using the inter-salt shale samples, the re-crystallization seepage tests, rock mechanical tests under high temperature and pressure, salt rock creep tests, and direct shear tests were conducted. The testing results suggest several major factors that affect hydraulic fracturing effects in the end. First, the seepage of reservoir and fracturing fluid through hydraulic fractures leads to salt dissolution and crystallization, reducing the effective seepage area of fractures. Second, the salt crystal may block the pore throats or micro fractures after brine invades the shale, decreasing the overall permeability. Third, the low strength and obvious plasticity of inter-salt shale and the strong creep characteristics of salt rock raise difficulties for proppant to effectively support fracture walls, thereby sharply narrowing the hydraulic fracture width. Lastly, the weak interfaces (bedding planes and lithology interfaces) in inter-salt oil shale reservoirs restrict the height of hydraulic fractures, resulting in the disconnection of seepage channels between multiple inter-salt shale reservoirs. Thus, several factors together reduce reservoir permeability, weaken the fluid flow capacity in the fracture, narrow the fracture width, and limit the effective stimulation volume, resulting in weaken the effect hydraulic fracturing.

1. Introduction

Organic-rich shale is an important and unconventional hydrocarbon resource, which consists of fine-grained sedimentary rocks containing large quantities of natural gas or oil (Boyer et al., 2011; Slatt, 2011; Barati and Liang, 2014). Shale typically serve as the source, reservoir, and seal of the hydrocarbons produced from them. Natural gas or oil is trapped in shale reservoirs; thus, shale is characterized as a self-contained source-reservoir (Jarvie et al., 2007; Slatt, 2011; Melikoglu, 2014; Yang et al., 2014). Accordingly, horizontal drilling and hydraulic fracturing must be adopted to achieve economic benefits because of the low to ultra-low permeability of shale players (Golding et al., 2013; Vengosh et al., 2013; Jackson et al., 2014; Li et al., 2018). Shale oil refers to liquid hydrocarbons existing in free, dissolved, or adsorbed states in the effective source rock of mudstones or shales (Jiang et al., 2016). Continental shale oil is a strategic onshore oil replacement resource with the highest potential in China (Hu et al., 2020). Shale oil in China is mainly distributed in the Permian strata of the Junggar Basin and Santanghu Basin, Triassic strata of the Ordos Basin, Jurassic strata of the Sichuan Basin, Cretaceous Songliao Basin, Paleogene in Bohai Bay, and Jianghan Basin (Hou et al., 2017; Wang et al., 2019; Zhi et al., 2019; Hu et al., 2020; Zou et al., 2020). In 2015, the Energy Information Administration (EIA) estimated that the technical recoverable resources of shale oil in China were 43.7 billion tons. The same statistic, which is reported by China Petrochemical Corporation (Sinopec), in 2019 stated that China's shale oil production was 7.4 billion to 37.2 billion tons. Meanwhile, China

* Corresponding author. State Key Laboratory of Geomechanics and Geotechnical Engineering, Institute of Rock and Soil Mechanics, Chinese Academy of Sciences, Wuhan, 430071, Hubei, China.
E-mail address: ytguo@whrsm.ac.cn (Y.-T. Guo).

https://doi.org/10.1016/j.petsci.2023.01.002

National Petroleum Corporation (CNPC) assessed China's technical recoverable resources of shale oil as 14.5 billion tons (including oil shale) (Hu et al., 2020; Zou et al., 2020). According to the "China Mineral Resources 2020" issued by the Ministry of Natural Resources of China, three parameter wells drilled in continental shale oil formations in Songliao Basin obtained a daily output that exceeded 10 m^3 of daily industrial oil production after the hydraulic fracturing of the shale in the section of Qingshankou Formation (Ministry of Natural Resources 2020). Thus, it demonstrates significant prospects for exploration and development of shale oil.

According to Li X.-E et al. (2019), a shale oil layer located between two salt layers is termed as "inter-salt shale". In the present study, a geological structure comprising a "salt layer-shale layer-salt layer" arrangement is termed as a rhythm; i.e., each rhythm is composed of organic-rich sedimentary rocks (sandstone, shale and carbonate) that are developed between salt layers. There are 193 sets of salt-bearing rhythms developed vertically in the Qianjiang Formation, among which shale and argillaceous dolomite are highly efficient as high-quality inter-salt hydrocarbon source rocks (Hou et al., 2017; Li et al., 2018). It has been reported that in the Qianjiang Depression, oil or gas is present in 32 out of 58 rhythms of inter-salt shale layers from Qian 2 to the upper section of Qian 4. Oil and gas are observed in 128 wells, out of which 32 are wells that can produce by formation pressure. Three wells exhibited strong blowout, thereby showing good prospects for exploration and development (Wang, 2015). However, the application of conventional reservoir stimulation methods to oil shale formation is not effective in the Qianjiang Depression where salt rhythms highly develop. Hydraulic fracturing was implemented in a directional well (Wangyun3 Well #7-2). However, the open hole section of the Well Wangyun11 was hydro fractured at 1667.56–1716.4 m using brine, and the fluid production rate dropped rapidly 10 days after fracturing (Wang, 2015). In addition, the pressure did not drop after the fracturing pump stopped, resulting in an unusual phenomenon (Han et al., 2016). Based on the practical on-site conditions mentioned above, the salt possibly dissolves and recrystallizes during the process of fracturing and production in this area. As a result, the high creep deformation of salt layers is obvious, which leads to a short effective period of high conductivity fractures and a fast decline in production (Jin, 2020). The existence of salt layers results in a different reservoir stimulation and dissimilar production characteristics of inter-salt shale reservoirs as compared to those observed previously. Salt minerals have a major impact on the hydraulic fracturing outcome of oil shale formations between the salt layers, which lead to the idea that the conventional fracturing method is not completely compatible with fracturing operations under special geological conditions. Therefore, it is important to carry out a research on the dissolution and crystallization of salts, rock mechanics of inter-salt shale reservoirs under the impact of temperature and pressure, and influencing factors of hydraulic fracturing of inter-salt shale layers.

In view of the special geological characteristics of inter-salt shale reservoirs, some researchers have conducted a significant number of studies recently. Bayram and Bektasoglu (2020) provided a statistical model to predict the actual dissolution rates by rock properties, such as compressive and tensile strengths, Poisson's ratio, cohesion, and experimental vertical dissolution rates. Yang et al. (2020) conducted salt dissolution and imbibition experiments, and high-temperature and high-pressure nuclear magnetic resonance (NMR) tests for inter-salt oil shale layers in Jianghan Basin to study the influence of salt dissolution in oil-bearing shale cores on spontaneous imbibition and permeability. Wanyan et al. (2019) analyzed the effects of the contents of different saline minerals (NaCl, Na_2SO_4, and $CaSO_4$) in salt rocks, concentrations, dissolution angles, and flow rates on dissolution rates by means of their established artificial neural network model for the dissolution characteristics of layered salt rocks. Yin et al. (2019) found that the formation temperature, pressure, and saturated brine can promote the self-healing ability of salt rock. First, the healing mechanisms include the purely mechanical closure of cracks due to elastic deformation and plastic flow. Second, diffusive or chemical crack healing driven by surface energy reduction is implemented. Third, cracks are healed by re-crystallization. Ma et al. (2015) studied the effects of temperature, pressure, and fluid flow rate (rotational speed) on the crystallization rate of salt rock, with regard to the process of salt deposition on the wellbore during oil recovery. Their study pointed out that the brine has a high crystallization rate only when the formation temperature is high and the flow rate is slow. Moreover, the pressure has little effect on the crystallization rate. For the mechanics of inter-salt shale or salt rock, Hou et al. (2017) investigated the geochemical, petrographic, and physical characteristics of saline shale from the Qianjiang Formation, such as organic matter type, thermal maturity, mineral composition, porosity and permeability features. Fan et al. (2019) evaluated the brittleness of the inter-salt shale from the Qianjiang Formation and found that the inter-salt shale is rather anisotropic and heterogeneous due to bedding planes and glauberite, while the inter-salt shale is semi-brittle at a high level of confining pressure. In addition, complex fractures are difficult to generate during hydraulic fracturing because of its obvious ductility. Guo et al. (2012) studied the mechanical properties of the Qianjiang salt rock under complex stress paths and found that salt has no obvious destruction surface even when subjected to large deformations under triaxial compression conditions. Li H. et al. (2019) analyzed the Qianjiang salt rock by using two-dimensional Particle Flow Code (PFC2D) to elucidate the deformation response, strength characteristics, and micro-cracking behavior under varying heterogeneity and different confining pressures. Liu et al. (2020a) investigated the impact of different types and contents of impurities on the mechanical properties of man-made salt rock, including density, strength, elastic modulus, Poisson's ratios, brittleness, and ductility. Finally, it was reported that the entire ductility of the rock salt would not be significantly impacted if the impurity content was low, such as within 50%. Time-dependent deformation behavior or creep is an important property of salts (Singh et al., 2018b). Li et al. (2020) numerically simulated the creep deformation of the Qianjiang salt rock by considering the deviatoric stress and temperature levels. Taheri et al. (2020) found that the time-dependent creep of Gachsaran rock salt exhibits a strong sensitivity to temperature change, while showing a low sensitivity to variations in differential stress. Mansouri and Ajalloeian (2018) found that increasing the axial stress level in creep tests resulted in more intensive creep deformation and a greater creep rate. In addition, for the topics related to underground salt caverns, several researchers have focused on the different stress loading/unloading paths and patterns of cyclic loading on the mechanical properties of salt rock (Fuenkajorn and Phueakphum, 2010; Fuenkajorn et al., 2012; Liang et al., 2012; Ma et al., 2013; Khaledi et al., 2016; Han et al., 2021; Wang et al., 2021). Most studies have demonstrated that salt rocks creep easily and dissolve, and the dissolution rate and deformation ability are more or less related to the ambient temperature, confining pressure, impurities, and other factors.

The aforementioned studies mainly focused on the dissolution, crystallization process, and mechanical properties of salt rock itself, while mostly are related to the construction of underground salt caverns. Thus, less attention has been paid to the relationship between the characteristics of salt rock and the sharp decrease in well production after hydraulic fracturing in inter-salt oil shale reservoirs. Under the special geological background of the Qianjiang Depression, salt rhymes are frequently deposited. Based on

laboratory tests, this study comprehensively considered the dissolution and crystallization factors, as well as the capacity of plasticity and creep of salt rocks in inter-salt oil shale reservoirs.

2. Geological background

China's continental lake basins comprise two types of source rock development environments: freshwater and saltwater (Hu et al., 2020). The Jianghan Basin is a typical saltwater saline lacustrine basin located in eastern China and covers 63360 km^2. It consists of five separate depressions from west to east, namely: Jiangling, Qianjiang, Mianyang, Xiaoban, and Yunying (Fig. 1a and b) (Philp and Fan, 1987; Wang et al., 2020). Rich shale oil resources formed within it under the unique sedimentary background of the continental saline lacustrine basin. The Qianjiang Depression, which is located in the middle of the Jianghan Basin and covers approximately 2500 km^2, contains the most hydrocarbon resources in this region, and it is the deposition center of the Jianghan Basin (Fig. 1b). In fact, the Qianjiang Formation contains the main oil-producing source rocks and reservoirs in the Qianjiang Depression (Zhang et al., 2003; Wang et al., 2020). The Qianjiang Formation is a set of salt-bearing strata that comprise four groups from top to bottom (Eq1, Eq2, Eq3, and Eq4), within which salt and inter-salt shale layers have been deposited by turns. The sedimentary thickness of the Qianjiang Formation from Eocene to Oligocene in Paleogene goes up to 4500 m, including 193 salt layers, i.e., 193 aforementioned “rhythms”. In addition, the cumulative thickness of rock layers goes up to 2000 m, and salt layers with a thickness greater than 10 m account for about 50% of the total thickness of the Qianjiang formation (Fang, 2002; Hou et al., 2017; Huang, 2018). As shown in Fig. 1c, from northwest to southeast, the three sediment units in the Qianjiang Formation were classified as the northern delta and fresh water facies, southern cyclotherm of saline facies, and middle transitional facies of brackish to saline water. Delta/fan delta facies developed along the northern border of the Qianbei Fault. The rhythms of alternating deposition of mudstones, thick halite and gypsum is the main characteristic of the middle to southern areas, while the lithological assemblage in the delta sedimentary area (yellow area in Fig. 1c) is interbedded deposit between sandstone and mudstone. In addition, the lithological assemblage in the brackish lake sedimentary area (blue area in Fig. 1c) is interbedded deposit between carbonate rock or thin-bedded sandstone (Wu et al., 2013; Hou et al., 2017). The halite strata are the result of the water desalination period; thus, large areas of organic-rich shale were deposited under deep-water conditions, resulting in a strong reducing environment. Due to the sheltering effects of the upper and lower salt layers, the shale oil generated from the inter-salt shale has difficulty migrating longitudinally and remains in the source rocks, thereby forming a unique inter-salt shale oil system (Sun et al., 2020).

3. Experiment

3.1. Sample preparation

As shown in Fig. 2, the samples involved in the present study were all extracted from the underground cores of the Qian 3 and Qian 4 formations of the Qianjiang Depression, Hubei Province. There are two types of shale: one is carbonaceous shale in deep black, and the other is a gray shale, which contains less organic matter; the thin interlayers of glauberite are clearly visible from the rock cores with well-developed bedding planes. Few bedding planes are debonding after coring out for a certain period of time; a certain portion of coring rock is pure salt rock, shale developed between salt layers, with clearly distinct interface between salt and shale (Fig. 2a). Considering dissolution of salt rock in water, all the samples for the experiment were cut with a diamond wire saw (Fig. 2b). There are cylindrical samples with a diameter of 25 mm and a length of 50 mm, cubic samples with the side length of 50 mm (Fig. 2c). The main mineral composition of the shale is albite (69.37%), dolomite (9.78%), illite (8.27%), and calcite (6.89%). The content of quartz (3.01%) was lower, and a small amount of pyrite (2.01%) and salt (0.66%) was present in shale. The salt rock mainly contains salt (92.49%), with a small amount of glauberite (5.17%) and gypsum (2.34%), as shown in Fig. 3a. A scanning electron microscope (SEM) test was carried out on the sample taken from the shale salt lithological interface (Fig. 3b). The electron microscope photos displayed a large salt crystalline grain, with tightly

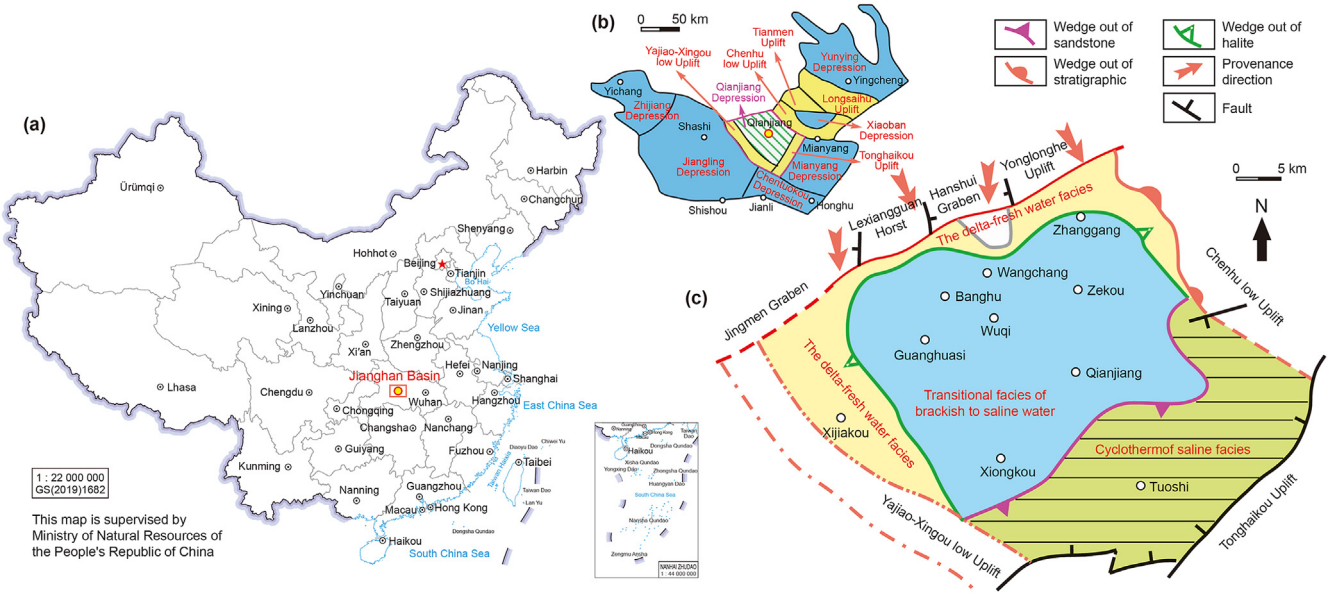

Fig. 1. (**a**) Location of the Jianghan Basin in China, (**b**) Qianjiang Depression in Jianghan Basin, and (**c**) sedimentary facies division of Qianjiang Depression. (This figure has been reproduced after referring to the study by Hou et al. (2017)).

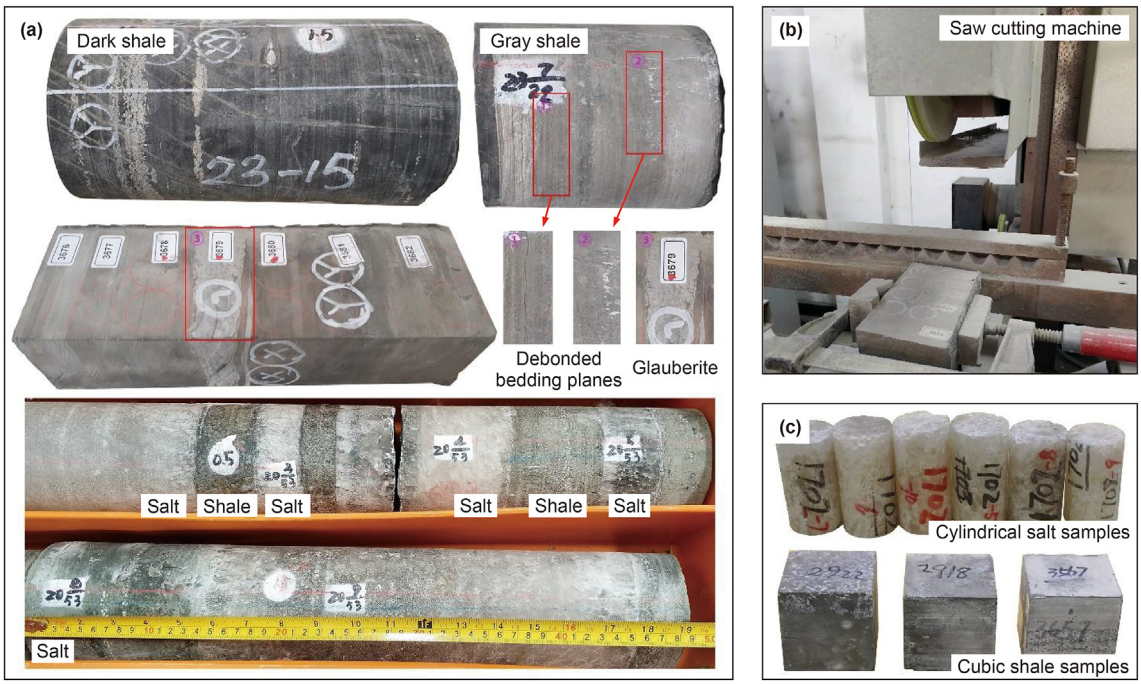

Fig. 2. (**a**) Photos of the shale and salt cores drilled out from Qianjiang Formation, (**b**) process of saw cutting, and (**c**) parts of cylindrical salt samples and cubic shale samples.

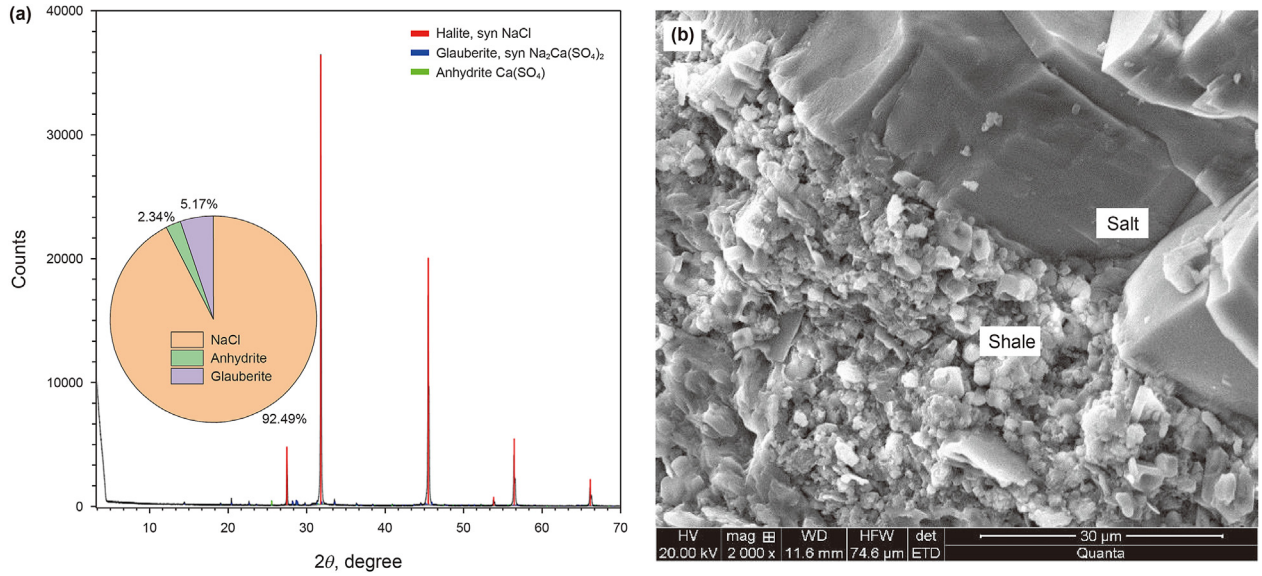

Fig. 3. (**a**) Energy spectrum of a salt sample and (**b**) scanning electron microscope (SEM) image of shale-salt lithological interface.

cemented salt rock-mudstone interface. However, the inter-crystalline cracks were found within the salt crystal grains, and numerous micro pores were present within the shale region. The basic parameters of the samples are listed in Table 1.

3.2. Experimental setup

The salt rock dissolution test was carried out in a water bath at temperatures of 20, 35, 50, 65, 80, and 95 °C. Before the test, the samples were dried at 105 °C for 24 h and then weighed for testing. The initial mass of the sample was determined, while the mass of the remaining sample was measured at certain time intervals during the dissolution process and the concentration of the solution at different times was calculated.

To simulate the long-term seepage process of saturated brine under the conditions of formation temperature and pressure, the Wuhan Institute of Rock and Soil Mechanics, Chinese Academy of Sciences, independently developed a simulation experimental system of salt rock recrystallization and seepage (Fig. 4), which consisted of an injection model and heating systems. It is composed of an automatic control system and a data acquisition and processing system. Upstream, saturated brine was injected into the core through a constant flow pump. The maximum pump injection pressure was 40 MPa, and the injection flow range was 0.01–10 mL/min. The constant-flow pump is first connected to the intermediate container through a high-pressure pipeline, and the intermediate

Table 1
Basic parameters of partial samples for experiments.

Test	Sample No.	Lithology	Diameter, mm	Height, mm	Weight, g	Density, g/cm^3
Salt rock dissolution test	1702–3	Salt	24.40	49.65	50.18	2.16
	1702–4		24.61	48.96	50.17	2.15
	1702–5		24.75	48.03	50.31	2.17
	1702–6		24.60	48.78	50.38	2.17
	1702–7		24.68	45.52	49.92	2.29
	1702–10		23.35	50.67	50.04	2.31
Recrystallization test	3763	Shale	25.91	45.80	57.80	2.39
	868		25.72	46.90	58.50	2.40
Multistage creep test	13 (63/74)	Salt	100.10	300.13	–	–
	25 (10/60)		100.05	400.20	–	–

container is connected to the core holder. The core holder can accommodate a core with a size of $\phi 25 \times 100$ mm; subsequently, the confining pressure (up to 50 MPa) was applied to the core through the ring pressure pump. The downstream of the core holder is connected to a back pressure valve, a back pressure pump, and a piston buffer container. The saturated brine flowing through the core holder was finally discharged into a beaker placed on a high-precision electronic balance (accuracy: 0.001 g) to obtain the flow rate of the saturated brine flowing through the core. The upstream intermediate container, core holder, and connecting pipeline between the two are wrapped by a heating jacket or a heating belt. The heating temperature was controlled by a temperature controller with a control accuracy of ±1 °C, and the maximum temperature recorded was 120 °C. The pressure and flow data were automatically collected and stored using the data acquisition system.

The experimental process is as follows: (1) Drying the samples under the temperature of 60–65 °C for at least 24 h, the rock samples shall be weighed every 8 h during the drying process. When the difference between two weighing is less than 10 mg, record the samples' weight. (2) Measure the geometric dimensions of rock samples, i.e. length and diameter. (3) Fully fill all the liquid-storage containers, pipelines and pumps, and ensure the brine is sufficient throughout the experiment process. (4) Put one shale samples into the core holder, screw tightly the plug of the core holder to fix the shale sample. (5) Turn on the valve of the confining pressure pump, and manually rotate the operating wheel to exert confining pressure, turn off the confining pressure valve when the preset value is reached. (6) Apply back pressure in similar operations to Step 5. (7) Turn on the temperature controller and set the testing temperature equals to reservoir temperature, the temperature controller automatically controls the temperature of the core holder through the heating jacket. (8) When the confining pressure, back pressure, and temperature reach the required values, turn on the constant flow pump valves, and set the high-precision balance to zero. (9) Activate the data collection button on the control system. (10) When the downstream pressure of the core holder does not change significantly anymore, stop the test.

The uniaxial and triaxial tests under high-temperature conditions were carried out on the XTR01 rock mechanics testing system, which can provide maximum 2000 kN in axial load, 150 MPa in axial pressure, 80 MPa in confining pressure, 100 mm in axial displacement, and 180 °C in temperature. The salt rock creep experiment was carried out on an RC-2000 rheological mechanics testing system, the control system was an all-digital servo controller named DOLI EDC-220. The rigidity of the loading frame is greater than 10 GN/m, maximum axial pressure is 2000 kN, maximum confining pressure is 70 MPa, and control error is less than 0.1%. Uniaxial and triaxial compression test, the muti-stage creep test are relative conventional, their testing procedures are not described here anymore.

4. Results and analysis

For inter-salt shale oil formation, when the formation fluid flows from the remote well area to the wellbore, there are at least two processes involving salt after fracturing. In the first process, the salt rock dissolves and saturated brine gradually forms during fluid seepage. In the second process, the formation fluid becomes saturated brine and carries NaCl to other locations in the formation. Under the influence of temperature and pressure changes, NaCl crystallizes. When the salt-shale-salt rock formation is connected by hydraulic fractures, the seepage paths alternatively cross through the salt and shale rock, and the dissolution of the salt rock mainly occurs within the area far from the well. In addition, the NaCl saturation of formation within the area near the well becomes increasingly high. Thus, there is only a dynamic equilibrium of dissolution, and the salt rock does not dissolve further. As the seepage velocity in the far well area is low, it can be regarded as an approximate static dissolution process. Therefore, a static dissolution test of salt samples under different temperature was first carried out to analyze the dissolution rate of salt. Then, an experiment of recrystallization in saturated brine was carried out to observe and analyze the recrystallization behavior of saturated brine that flowed through the fractures.

4.1. Dissolution of salt rock under different temperatures

Fig. 5 is a photograph of the salt rock sample (partial) after it was subjected to the static dissolution test at 95 °C. As the dissolution time increased, the length and diameter of the samples decreased. In the first 15 min, the appearance of the sample changed significantly; the sample surfaces turned rough and uneven and the length reduced by approximately 3 mm. Photographs of the residual salt samples after the dissolution test under various temperature conditions are shown in Fig. 6. The surface of the samples changed to different degrees, while becoming rough with increasing temperature; and the surface with more impurities (darker color implies more impurities) changed more severely.

Fig. 7 shows the relationship between the dissolved mass (m_d) and residual mass (m_r) of salt rock with time under different temperatures. The dark-colored area in the lower half of the figure is the percentage of residual salt mass, and the light-colored area in the upper half is the corresponding dissolved mass percentage. Temperature and dissolution time significantly affect the dissolution rate of salt rock. Taking 20 °C as an example, the percentages of residual mass at 5, 15, 25, 35, and 45 min to the total mass are 93%, 76%, 67%, 60%, and 54%, respectively. It can be inferred that the dissolved mass percentage within 5–45 min is 6%–8%, while the increased dissolved mass per 10 min measured from 55 to 65 min is 2%; apparently, the dissolution rate of the salt sample decreases significantly with time. Fig. 8 reveals that the salt dissolution rate is high in the initial stage, and the molar concentration of NaCl in the

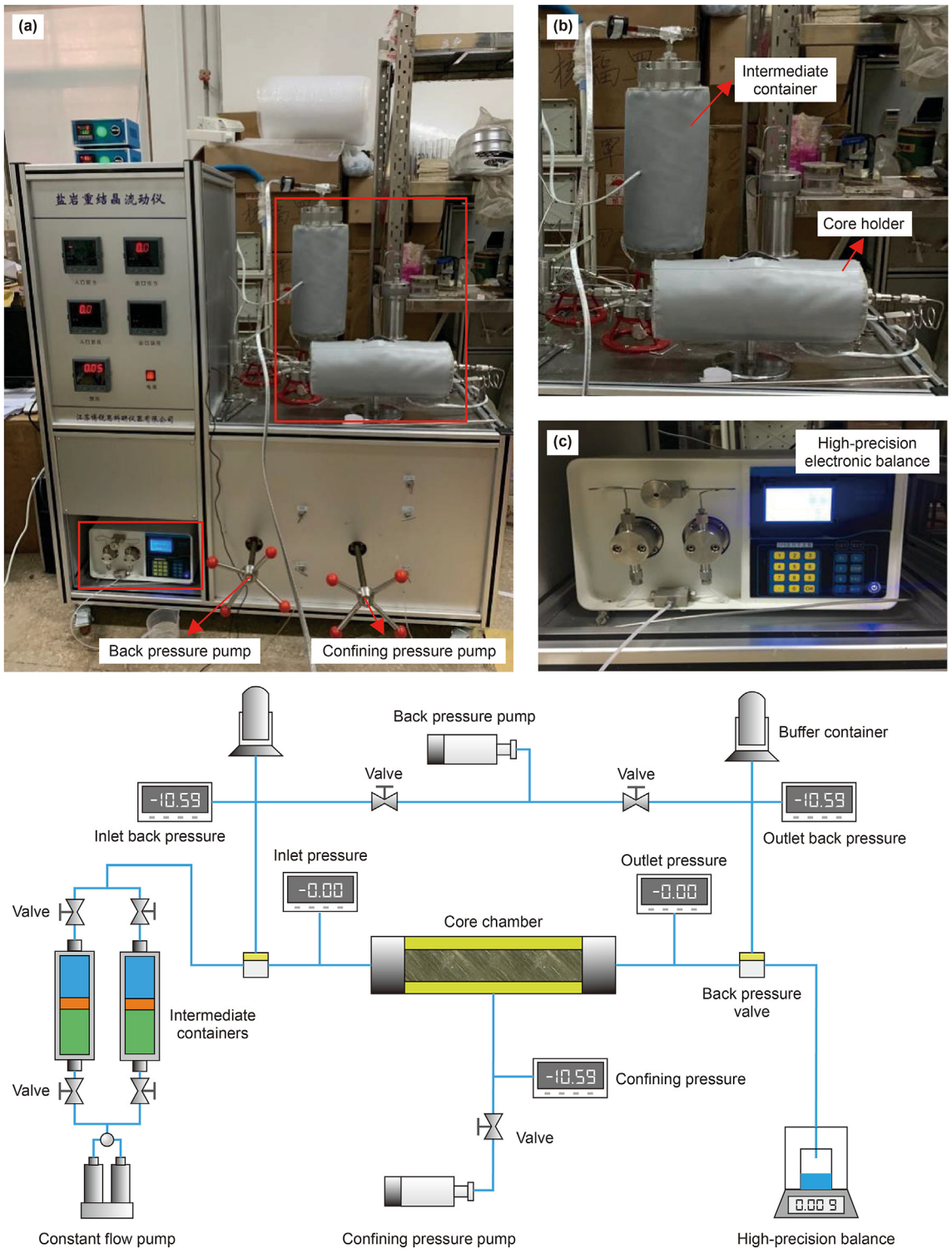

Fig. 4. (**a**, **b**, **c**) Experimental setup of salt rock recrystallization and seepage and (**d**) the schematic diagram of the recrystallization seepage testing equipment.

brine increased rapidly. At a later stage, as the dissolution time increases, the solution gradually becomes saturated; thus, the residual mass of the salt becomes constant, and the dissolution rate gradually tends to zero. Accordingly, the molar concentration of NaCl in the brine gradually stabilizes. In summary, a lower NaCl concentration in brine and a higher temperature lead to a higher dissolution rate of salt rock. When the temperature is higher, the final residual salt mass percentage is lower, and the NaCl molar concentration in the final solution is higher; i.e., the NaCl solubility in the final solution is higher.

4.2. Effect of recrystallization on fracture permeability in shale

4.2.1. Intrinsic fracture characteristics of shale

Fig. 9 displays CT slices of the inter-salt shale core samples with glauberite in the bright area. CT slices exhibit highly developed

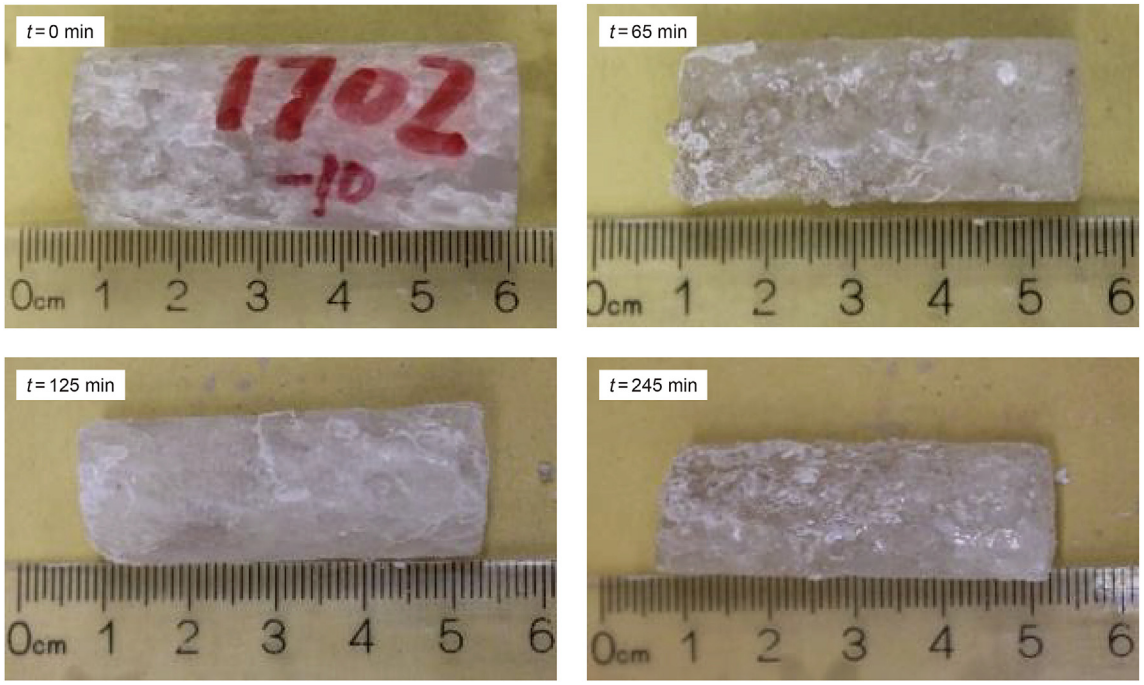

Fig. 5. Photographs of the salt rock sample (No. 1702-10) after different dissolution times at 95 °C, both the length and diameter reduced, and the core surface gradually became potholed.

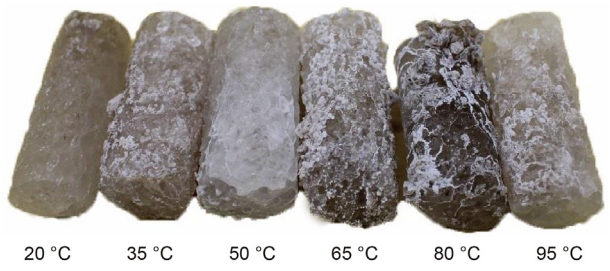

Fig. 6. Photos of salt rock after dissolution under different temperatures. The sample surfaces after dissolution became rough and more impurities (with darker color) seem to exacerbate this change.

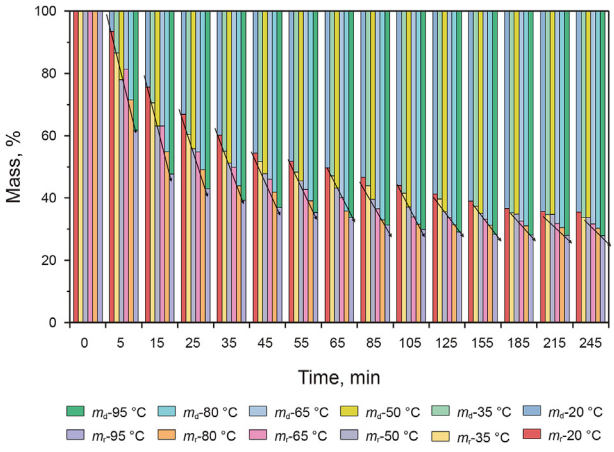

Fig. 7. Dissolved mass (m_d) increased sharply in the early time but gradually kept unchanged in the end, higher temperature leads to more dissolution of salt rock, and residual mass (m_r) shows an opposite trend.

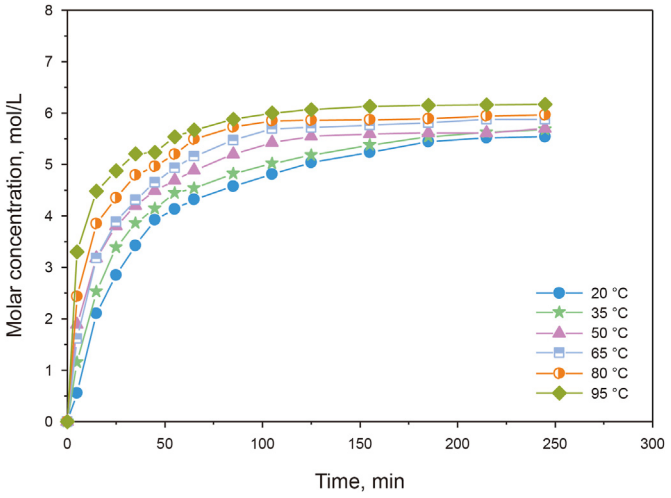

Fig. 8. Solution concentration initially increases with time and then remains stable in the later time stages under a certain temperature. A higher temperature leads to a greater dissolution rate of salt at the initial stage and higher molar concentration of NaCl at the end.

abundant natural bedding fractures in the shale samples. The width of the natural fractures in shale sample #3763 ranges between 50 and 180 μm, while the width of sample #868 lied between 100 and 250 μm. The fractures are distributed continuously or discontinuously through the entire core cross-section, and several micro fractures can be observed. All bedding planes are roughly parallel. In addition, the direction of the bedding cracks changes within the area of glauberite development, along with the emergence of some micro cracks that are perpendicular to the bedding cracks. The fully developed micro-fractures in the core provide seepage channels for

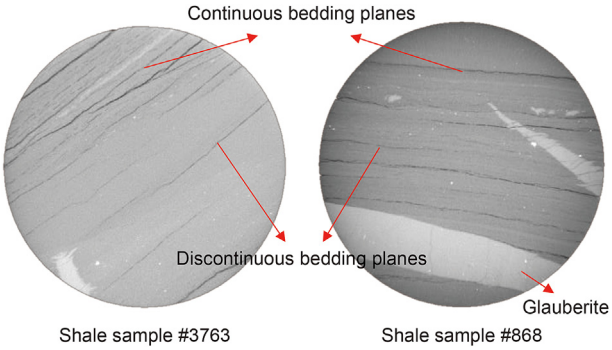

Fig. 9. Highly developed natural fractures in the CT images of shale samples #3763 and #868.

formation fluids and simultaneously provide space for NaCl crystallization when saturated brine flows through it.

4.2.2. Influence of recrystallization during brine seepage in shale fractures on permeability characteristics

Before the experiment, the upstream intermediate container, shale sample, and core holder were fully heated using a heating jacket. After reaching the predetermined temperature, the confining pressure was increased to 20 MPa, the upstream back pressure was controlled to be approximately 13 MPa, and the lower back pressure was set to 2 MPa. Other experimental parameters are listed in Table 2. The fluid mass through the core was measured by an electronic balance, and the permeability was calculated based on Darcy's law.

Fig. 10a demonstrates that for sample #868, when the temperature difference between the saturated brine and sample is 30 °C, the seepage process can be divided into three stages according to the change pattern of inlet pressure and permeability. Stage I: The inlet pressure and permeability drop rapidly in a short time; Stage II: The inlet pressure remains constant and the permeability drops slowly; Stage III: The inlet pressure rises slowly, and the permeability continues to drop slowly. The reason for the rapid decrease in inlet pressure and permeability in Stage I is that the initial fractures of the core are relatively wide, as shown in the CT images in Fig. 9. Here, the primary fractures begin to close quickly at the initial stage after the confining pressure is exerted; thus, the permeability also shows a rapid downward trend. However, in Stage I, primary fractures are not completely closed, while the fractures still have a certain degree of opening and the fluid seepage velocity is still relatively fast; therefore, the inlet pressure initially decreases quickly. When the seepage process enters Stage II, the inlet pressure gradually stabilizes, and the permeability gradually decreases steadily at a relatively small rate. To a certain extent, the reason for these results may be reduction in the width of the larger primary fractures at this stage. The micro-fractures are also closed, the overall width of the original fractures tends to be stable, and seepage velocity is greatly reduced and reaches a stable value. At this stage, due to the temperature variation of the saturated brine, NaCl crystals may have begun to be produced on the inner wall of the fractures in shale with a decrease in seepage rate. The seepage process enters stage III when the testing time is approximately 500 s. The number of NaCl crystals increases with an increase in the crystal volume; thus, the cracks are partially blocked, and the inlet pressure begins to rise. Accordingly, the permeability continues to maintain a downward trend.

The same test with a temperature difference of 70 °C was carried out for sample #3763. It can be seen from Fig. 10b that in stage I of this test, there is no significant difference in the varying pattern of inlet pressure and permeability between the conditions of 30 and 70 °C. As the test time increases, both the inlet pressure and permeability of the shale sample decrease rapidly. In Stage III, the inlet pressure rises slowly, whereas the permeability decreases slowly at a small rate. The difference lies in the fact that, after the temperature difference reaches 70 °C, the inlet pressure slowly drops or remains constant, and the permeability drops by an unapparent speed in Stage II. When Stage I ends at a percolation time of approximately 100 min, it directly enters Stage III. Furthermore, in Stage III, the amplitude and rate of increase in the inlet pressure of sample #3763 are significantly higher than those of sample #868. The above difference mainly arises due to the increase in the temperature difference between the saturated brine and the core, as well as the quick precipitation of NaCl and adherence to the crack wall due to the flow of saturated brine through the shale core. The large temperature difference accelerates the growth of salt crystals, which leads to an earlier time point for the rise in inlet pressure, and an increase in the rate and amplitude of the inlet pressure.

4.2.3. Position of NaCl crystallization and morphology in the shale fractures after the tests

Fig. 11 exhibits photographs of samples #868 and #3763 after recrystallization. After unloading the confining pressure and taking out the sample, the shale sample cracked along the natural sedimentary bedding. It can be observed that there is a layer of white salt crystals attached to the surfaces of the bedding planes and the end faces of sample #868 (temperature difference is 30 °C). In addition, the number of salt crystals around the cracks at the end surface was observed to be significantly greater than the rest of the end surface. For sample #3763 (temperature difference is 70 °C), three bedding planes were cracked and opened after the end of the tests, revealing that the white salt crystals are distributed in clusters or narrow strips, which may be affected by the shape of the crack wall. Furthermore, the salt crystal grains gathered along the sedimentary plane on the end surfaces of the sample. Salt crystals were observed in the cracks and end faces of samples #868 and #3763, indicating that salt crystals precipitated out during the experimental process. Comparing the crystallization conditions of samples #868 and #3763, it can be observed that the number and degree of aggregation of salt crystals in the fracture and end surface of the shale core for sample #3763 are greater than those for sample #868, indicating that a large temperature difference promotes the precipitation of salt crystals. On the contrary, a small temperature difference can slow down the crystallization of NaCl when saturated brine flows through the bedding plane cracks. Comparing the inlet pressure and permeability curves of samples #868 and #3763, it can be observed that the higher the degree of salt crystal precipitation, the higher the inlet pressure during the recrystallization test.

As per the sample photographs obtained after testing, only the

Table 2
Experimental parameters of brine recrystallization in shale samples.

Sample No.	Confining pressure, MPa	Pumping rate, mL/min	Upstream temperature, °C	Temperature of shale sample, °C
3763	20.0	0.05	90.0	20.0
868	20.0	0.05	90.0	60.0

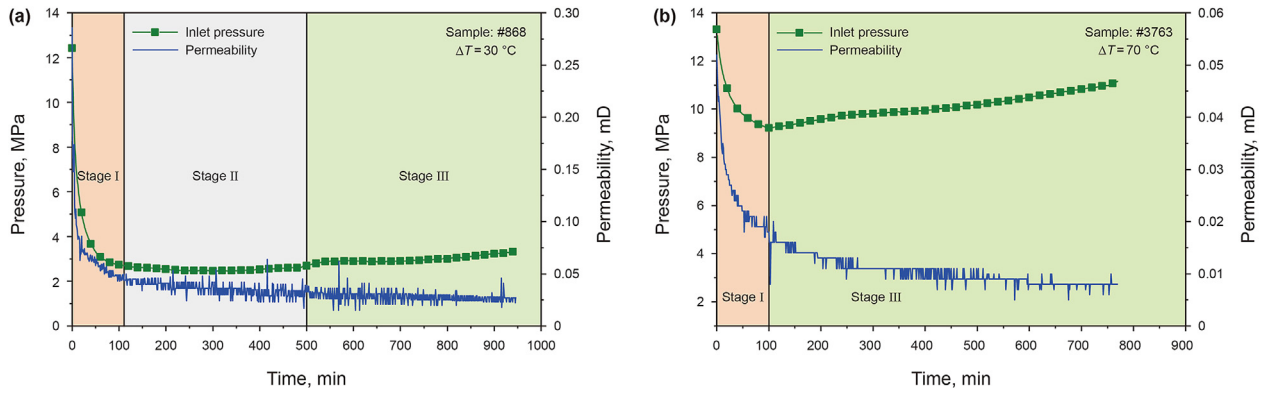

Fig. 10. Change in inlet pressure and permeability with testing time. The inlet pressure gradually rises with a slow decrease in permeability during brine recrystallization in fractures of the shale samples.

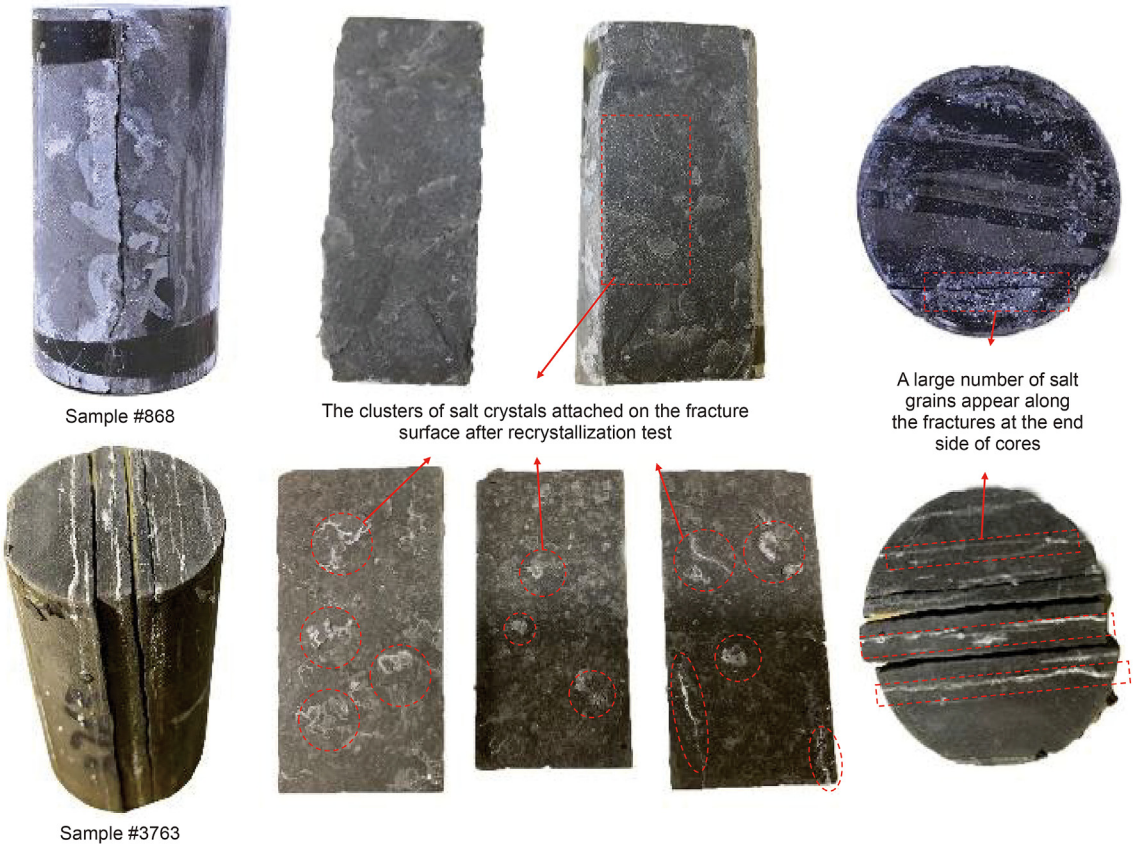

Fig. 11. Clusters of salt crystals appear along the fractures in shale samples after recrystallization tests.

macroscopic distribution of salt crystals on the surface of the core can be observed after testing. Scanning SEM can be used to observe the microscopic characteristics of the shale surface after NaCl crystallization. Simultaneously, EDX can perform qualitative and semi-quantitative analyses of the types and contents of micro-component elements. The elements of the attachments on the surface of the shale cracks were analyzed using EDX, and the results are shown in Fig. 12. The electron microscope photos exhibit the white matter attached to the micro-cracks, which developed in strips as a regular hexahedral crystal structure. The main elements of the white substances were Na and Cl. It is a known fact that the NaCl crystal has a hexahedral structure; thus, it can be concluded that the substance with regular structural characteristics under the electron microscope is NaCl crystal. The EDX results exhibited that NaCl was attached to the crack surface in irregular bands or clusters. On this basis, scanning electron microscopy (SEM) was used to observe the crystallization and distribution conditions of NaCl.

Fig. 13 shows the scanning electron microscope (SEM) images of the fracture surface in the shale samples, with small to large magnification. At a smaller magnification, as shown in Fig. 13a and b, it can be seen that there are clusters of white matter distributed near the micro cracks, and the EDX analysis of the clusters reveals that it contains a higher content of Na and Cl. This may be due to the interaction of brine with other substances in the micro cracks, such

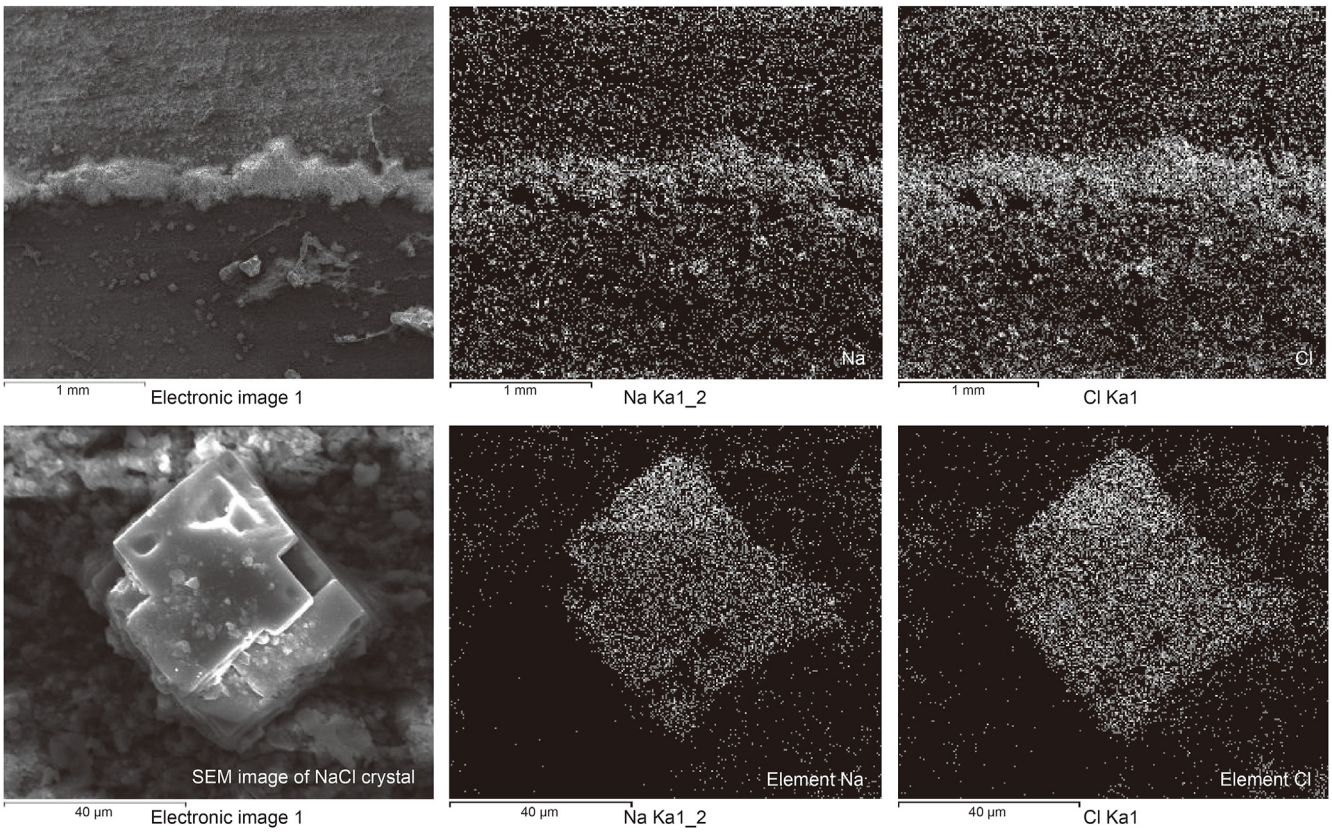

Fig. 12. Qualitative analysis results of EDX elements.

as clay minerals and other substances. Thus, tiny salt crystals adhere to these substances, appearing in the form of clusters. Under the electron microscope, some regular-shaped salt crystal grains are scattered on the surface of the cracks, which basically present a hexahedral shape with grain sizes mostly below 50 μm. In Fig. 13c, it can be observed that some incompletely formed NaCl crystals are attached to the crack wall in the form of quadrilateral flakes. Whether it is a flocculent substance attached to NaCl or a regular or irregular NaCl crystal, their existence will definitely reduce the seepage space in the original crack, increase the seepage resistance of the crack, and further reduce the fracture permeability. With a longer seepage time and higher seepage temperature difference, more salt crystals may be formed, and the initial cracks are filled by salt crystal grains. In addition, the incompletely formed salt crystal flakes are connected to each other to form a partial film-like salt crystal coat, which also blocks the throat of the fracture wall and affects the flow of fluid in the rock matrix into the fracture, thereby reducing the permeability of the shale matrix.

4.3. Salt rock plastic deformation and long-term creep effect

4.3.1. Mechanical properties of rocks under high temperature and high-pressure conditions for inter-salt shale oil reservoir

Rock mechanical tests of inter-salt shale and salt rock under high-temperature and high-pressure conditions were performed. Fig. 14 shows the stress–strain curves of the shale and salt rock. The basic parameters and test results for the samples are listed in Table 3. When the confining pressure of shale is 10 MPa, the elastic modulus is 12.1 GPa and Poisson's ratio is 0.16. the axial stress gradually decreased to residual strength when reached peak stress, the angle between the shear failure surface and the core axis is 45°. When the confining pressure reaches up to 50 MPa, the elastic modulus does not change significantly; however, Poisson's ratio increases to 0.29. When the confining pressure increases, the plasticity of the rock is obviously strengthened. Thus, the stress drops slightly after reaching its peak, exhibiting the characteristics of plastic flow.

However, the elastic modulus and Poisson's ratio of the salt rock sample containing inclusions and the pure salt rock sample were not significantly different. After the confining pressure increased from 10 to 50 MPa, the elastic modulus increased to twice that observed at a low confining pressure, and Poisson's ratio decreased to 1/2 of that at 10 MPa. The stress–strain curves reveal that the two salt rocks begin to dilate when the deviatoric stress reaches 10–15 MPa during the loading process, thereby causing plastic deformation. When the peak strain reaches a confining pressure of 10 MPa, the axial and radial strains of the salt rock-containing inclusions both reach up to 10%, and the axial and radial strains of pure salt rock are 13% and 10%, respectively. After the confining pressure is increased to 50 MPa, the peak stress does not reach within the test stress range. Except for the core YL3-2-3, the axial and radial strains of salt rock with inclusions and pure salt are both greater than 12%. In addition, for the Qianjiang salt rock, Guo and Cai (2010) carried out single triaxial mechanical tests under different temperatures and confining pressures. Their study also showed that salt rock in the Qianjiang area has high amount of softness and plasticity. Even under lower pressure, the plastic deformation of rock is extremely strong, and the higher temperature seems to result in a lower strength of the salt rock. The low elastic modulus and strong plastic deformation of the Qianjiang salt will lead to large plastic deformation of the salt layer during the process of hydraulic fracturing in salt layers, thereby resulting in a

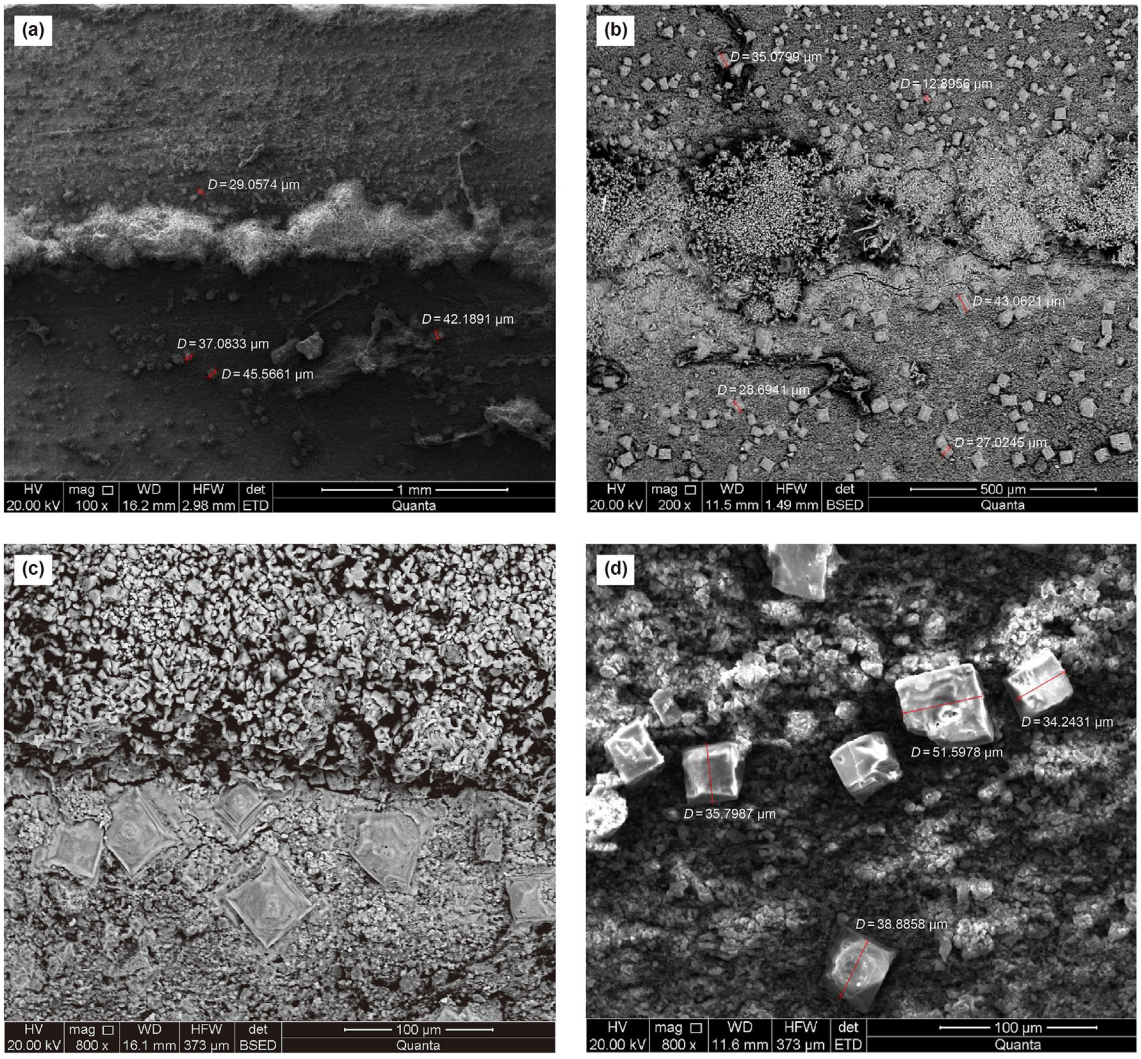

Fig. 13. SEM images of shale fracture surface. NaCl crystals are found at the fracture surfaces. The diameter ranges from 10 to 55 μm.

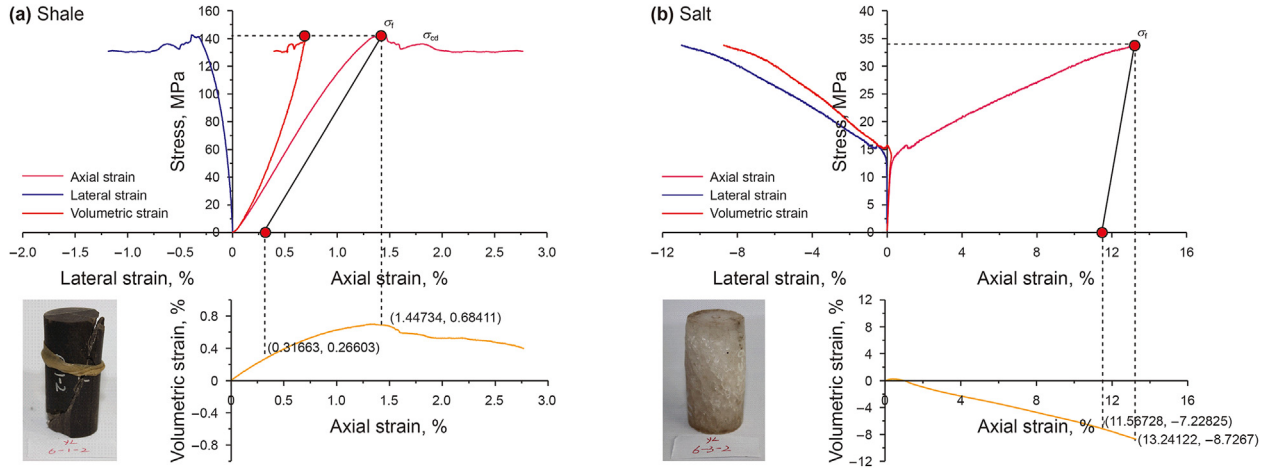

Fig. 14. Stress–strain curves under triaxial tests of shale (**a**) and salt rock (**b**). Both the curves of shale and salt indicate plastic deformation characteristics.

high local pressure and reducing the length scale of hydraulic fractures and the stimulation volume of inter-salt shale oil layers. At the same time, the strong plasticity of shale and salt rock will also cause serious embedding of proppant, thus leading to fracture support failure.

Table 3
Rock mechanical properties of shale and salt rock from inter-salt shale oil reservoirs.

Lithology	Sample No.	Formation	Diameter, mm	Height, mm	Density, g/cm^3	Temperature, °C	Confining pressure, MPa	Compressive strength, MPa	Elastic modulus, GPa	Poisson's ratio
Shale	YL6-1-a	Eq4	24.46	49.96	2.27	95	10	58.74	12.10	0.16
	YL6-1-2		24.52	48.84	2.37		50	192.50	12.02	0.29
Salt rock containing inclusions	YL3-2-1	Eq4	24.43	50.30	2.20	95	10	33.53	3.18	0.21
	YL3-2-3		24.46	49.92	2.21		50	76.33	6.94	0.11
Pure salt rock	YL6-3-a	Eq4	24.46	50.62	2.18	95	10	33.89	3.88	0.18
	YL6-3-2		24.46	51.38	2.17		50	78.79	7.21	0.11

4.3.2. Creep characteristics of salt rock under high-temperature and high-pressure conditions

Multi-stage creep tests were carried out on salt rock under the same temperature and confining pressure. When the creep curve is stable, the deviator stress (the difference between the axial pressure and the confining pressure) is used to obtain the creep rate under different deviator stress conditions. Tables 4 and 5 indicate the creep rates under different deviator stresses and temperatures. Fig. 15a shows the effect of deviatoric stress on the creep rate at 20 and 86 °C, and Fig. 15b shows the effect of temperature on the creep rate under the conditions of 10 and 15 MPa deviatoric stress. The creep rate of salt rock is affected by both the temperature and deviatoric stress levels. The higher the temperature, the greater the deviatoric stress, and the greater the creep rate. When the salt layer is fractured, the differential stress between the wellbore and the formation is relatively large, and the formation temperature is relatively high (80–120 °C), resulting in significant creep ability of the salt layer. Therefore, the salt layers may deform significantly and cause the fracture to close. The salt rock temperature near the wellbore decreases with the production of shale oil, and the salt deviator stress value decreases after salt deformation reaches a certain extent, thereby gradually weakening the creep stability of salt formation; however, the creep effect at the initial production stage has a greater impact on hydraulic fractures. Therefore, the strong creep effect of the salt layers should be considered during hydraulic fracturing design, such as selecting proppant with large diameters.

4.3.3. Shear mechanical properties of salt-shale interfaces

Shear testing can be used to obtain the mechanical properties associated with the shale interface of inter-halite shale. The shear plane was mostly observed to be along the bedding planes or lithology interface, while the shear strength was low and sample failure occurred at a small shear displacement (< 0.3 mm). For example, due to the failure along a lithology interface, as shown in Fig. 16a, the glauberite and shale sedimentary interface can be seen on the surface of sample #2448. Shear along the lithology interface forms a smooth shear surface after the shear test. In addition, some white substances can be observed at the shear surfaces, which presents a step-like cracking failure mode. White salt minerals are also found to be uniformly distributed on the interfaces; thus, it can be inferred that these deposits greatly reduce the strength of the bedding planes. As shown in Fig. 16b, the shear strength under different normal stresses is fitted, the cohesion strength of the bedding interface is 0.99 MPa, the internal friction angle is 32.01°, and the cohesion strength of the lithology interface is 0.74 MPa with an internal friction angle of 20.24°. Thus, it can be observed that the lithology interface and the bedding interface are both weak structures. When hydraulic fractures extend to these weak interfaces, they may likely deflect along these weak structures, even merely propagating along this sedimentary interface in the later process; this hinders the direction and height of the hydraulic fractures. It is difficult to effectively stimulate the shale layers, and when the bedding planes are opened, the large angle deflection of the fracture will affect the migration of proppant.

Table 5
Steady creep rate at different temperatures.

Temperature, °C	Confining pressure, MPa	Steady creep rate under different deviatoric stress levels, h^{-1}	
		10 MPa	15 MPa
50	10	2.6×10^{-5}	8.733×10^{-5}
75	10	3.247×10^{-5}	1.325×10^{-4}
86	10	5.19×10^{-5}	2.12×10^{-4}

5. Discussion

Based on the above test results, it is inferred that there are several major factors that decrease hydraulic fracturing effect. In summary, the main points are as follows.

5.1. Dissolution of multi-rhythm salt layers provides basis for NaCl crystallization

The recrystallization test mentioned in the previous section demonstrates that the phenomenon of crystallization in fractures does exist and causes the shale permeability to decrease. After shale formations are connected by hydraulic fractures, the formation water or residual fracturing fluid flows into the wellbore through the artificial fractures, which may be dissolved and crystallized repeatedly during this process, as shown in Fig. 17. The blue balls represent the NaCl dissolved from the salt rock, and the yellow

Table 4
Steady creep rate under different deviatoric stress levels.

Deviator stress, MPa	Confining pressure, MPa	Steady creep rate under different temperatures, h^{-1}	
		20 °C	86 °C
5	20	2.15802×10^{-8}	5.19×10^{-5}
10	20	5.72729×10^{-6}	6.12×10^{-4}
15	20	1.49912×10^{-4}	5.37×10^{-3}
20	20	1.52×10^{-3}	9.70×10^{-3}
25	20	9.17×10^{-3}	2.076×10^{-2}

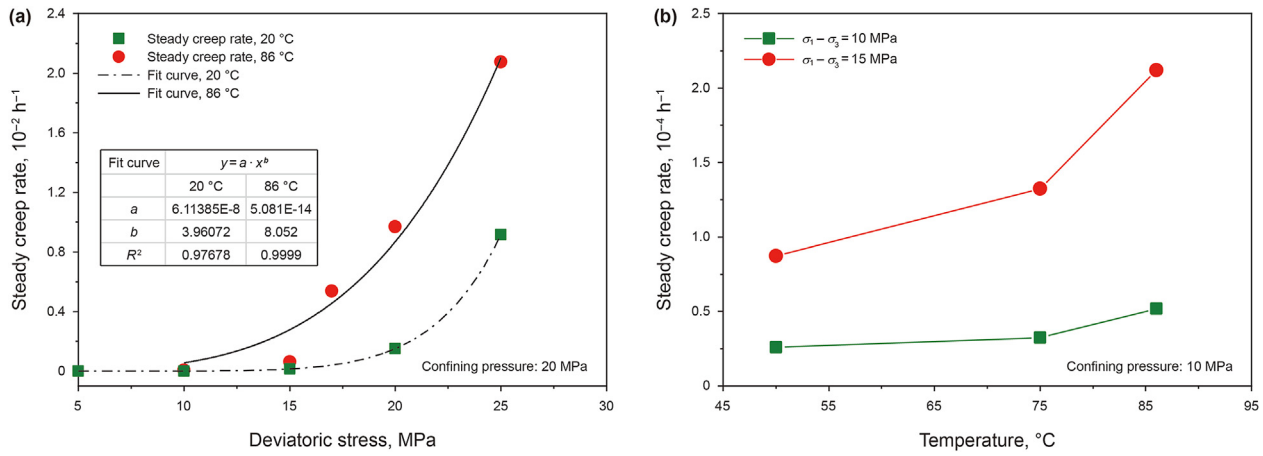

Fig. 15. Creep rate rises with the increase of deviatoric stress (**a**) and temperature (**b**).

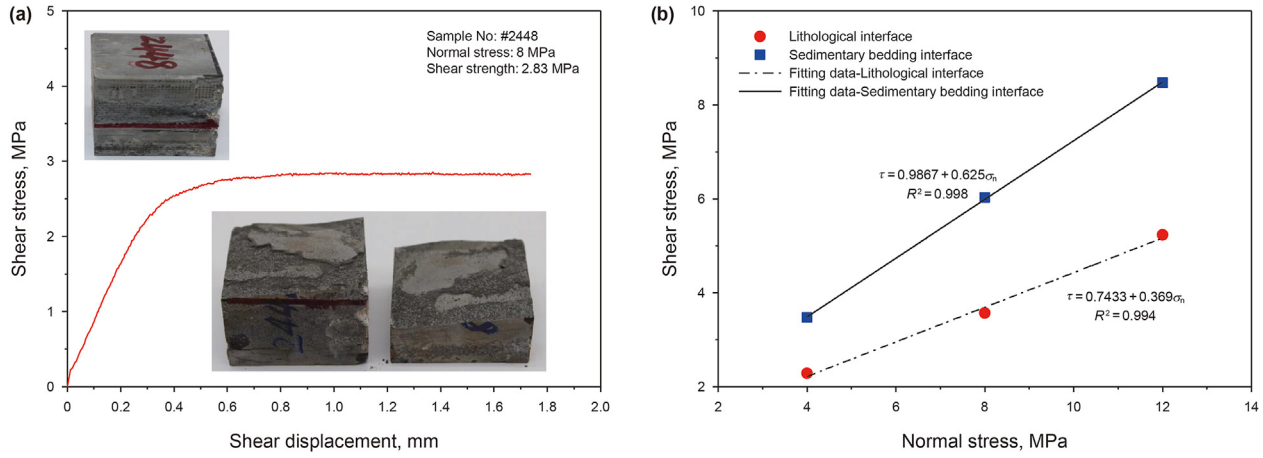

Fig. 16. (**a**) Photos of shale sample #2448 after shear testing and its shear stress–displacement curve. (**b**) The shear strength under different normal stress levels.

balls represent the transfer of NaCl back to the fracture surface during the dynamic dissolution by crystallization. Note that when NaCl dissolves in the fluid, it will exist as Na^+ and Cl^-; for brevity, the small ball is used in this diagram to generally represent it as NaCl. Within an area far away from the wellbore, the NaCl concentration in the formation fluid is low; thus, dissolution of the salt rock occurs. With an increase in the number of salt layers that the fluid travels through, the salinity also increases. In the near-well area, the brine reaches a saturated state, and the recrystallization of NaCl appears at both the fracture mouth and wellbore wall. The NaCl solution formed after three dissolution stages is the material basis for the subsequent crystallization phenomenon. Once the temperature or pressure of the solution changes, dissolution or crystallization of NaCl occurs.

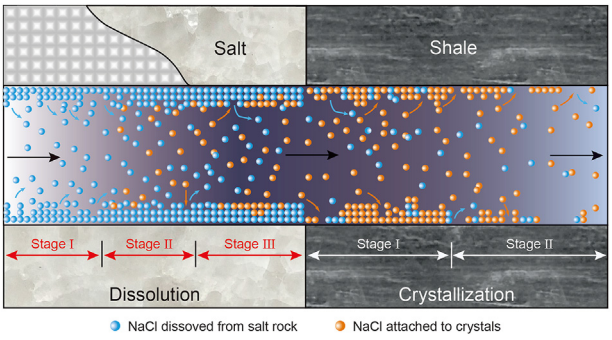

Fig. 17. Diagram of dynamic dissolution of salt rock and the recrystallization of NaCl along fractures. Salt starts to dissolve when the reservoir or fracturing fluid is unsaturated and NaCl recrystallizes when it flows through fractures in shale layers after the fluid is saturated.

5.2. NaCl recrystallization blocks pore throats and hydraulic fractures of shale

As shown in Fig. 18, when the formation fluid in hydraulic fractures flows through salt layers, NaCl dissolution occurs to form saturated brine. When it flows through the shale reservoir, NaCl precipitates under the influence of temperature and pressure and NaCl crystals grow on the fracture walls, thereby reducing the flow area of the fractures and increasing the flow resistance. On one hand, when the resistance in the fracture increases and the seepage velocity decreases, the lower flow rate is conducive to the further development of crystals. On the other hand, with the precipitation of NaCl crystals and the flow of stratum fluid along fractures, NaCl concentration gradually slows down the precipitation of crystals. When the fluid in the hydraulic fractures becomes unsaturated and flows through the salt rock formation, the aforementioned dissolution process repeats. In addition to the crystallization that occurs

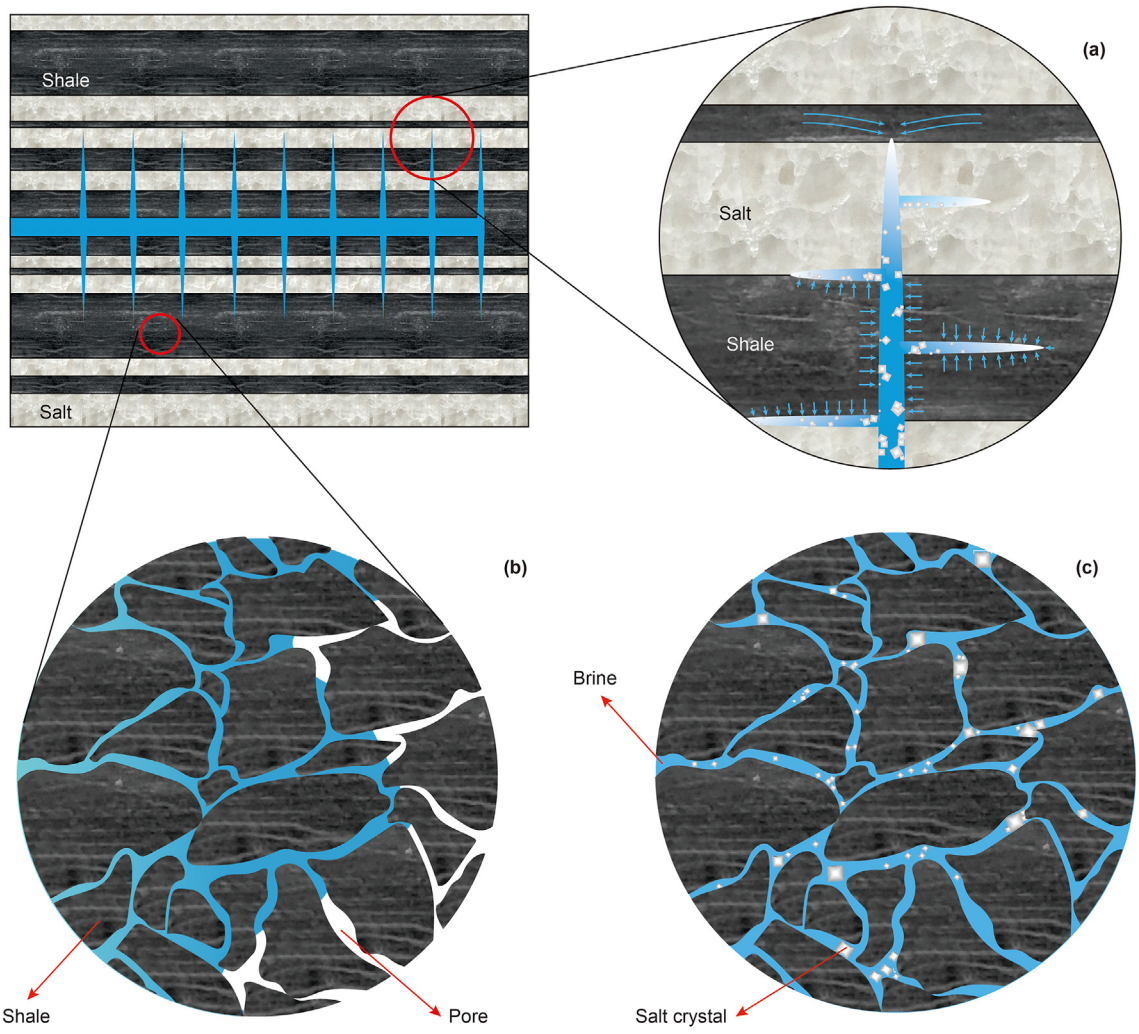

Fig. 18. Diagram of NaCl recrystallization in micro pores and hydraulic fractures.

within the hydraulic fractures described in Figs. 17 and 18a, the micro pores and micro cracks within the shale matrix may also block the pores and micro cracks in the matrix or on the crack wall due to salt crystallization (as shown in Fig. 18b and c), thereby reducing the overall permeability of the shale reservoir. The two aforementioned major reasons likely cause a reduction in the effective pores and fractures in the shale reservoir, thereby ultimately resulting in a sharp decline in productivity.

5.3. Plastic deformation and creep of salt rock led to proppant failure and fracture closure

The rock-mechanics testing results in Section 4.3 infer that the elastic modulus of inter-salt shale is low (approximately 12 GPa) and that the elastic modulus of impure and pure salt rocks was very low (less than 10 GPa), while the compressive strength was also very low. Many studies (Yang et al., 1999; Wang et al., 2011; Zhang et al., 2012; Ma et al., 2014; Mansouri and Ajalloeian, 2018; Liu et al., 2020b) have indicated that salt rock has a much stronger plasticity and creep stability than that of other rocks after hydraulic fracturing, owing to the strong plasticity of shale, especially the salt layers. Considering the strong creep of the salt itself, the rock in the surrounding artificial fractures is prone to plastic deformation and creep after hydraulic fracturing, resulting in the proppant being unable to effectively support hydraulic fracture surfaces. As shown in Fig. 19, when proppant support initially fails in the salt layers, the degree of proppant embedding in the fracture walls of the shale layers increases accordingly, and the overall fracture width decreases. Even after a period of time, the proppant may be completely embedded; thus, the hydraulic fractures will be completely closed. It is worth mentioning that, owing to the plastic deformation and creep of salt and the dissolution and crystallization in the fractures, the artificial fractures in the salt layer may self-heal (Fuenkajorn and Phueakphum, 2010; Singh et al., 2018a; Yin et al., 2019; Liu et al., 2020b). Therefore, the combination of various factors causes the originally connected inter-salt shale reservoirs to lose effective communication. As efficient seepage channels have been blocked in the end, the oil well production declines significantly.

5.4. Shielding and sealing effects of salt rock limit the stimulating volume of hydraulic fractures

Through the shear test in Section 4, it was found that the bedding planes or lithology interfaces inside the shale were weak structures, and the shear strength was very low. Therefore, as shown in Fig. 20, when the artificial hydraulic fracture tip reaches these interfaces, it causes dislocation on interfaces. Meanwhile, the

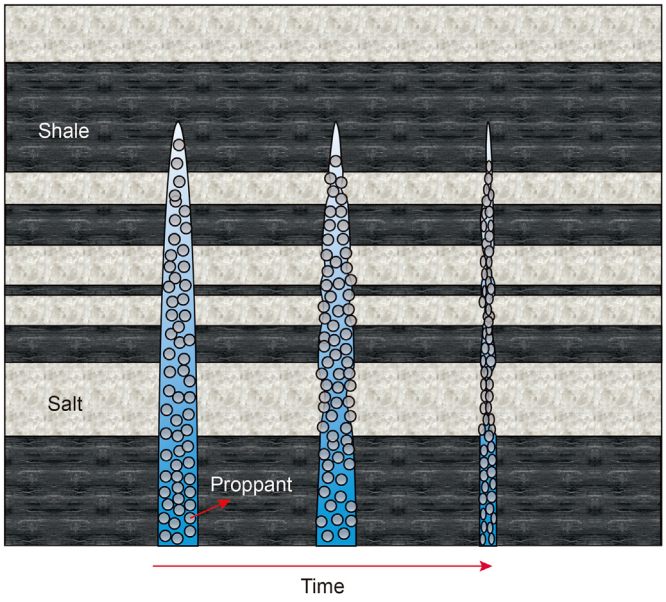

Fig. 19. Diagram of fracture closure due to proppant embedding into low-strength shale and salt. The plasticity and creep of salt also contribute to the fracture closure.

sedimentary surfaces or interlayer lithology interfaces in the shale layers tend to open and hydraulic fractures are propagated along those structures and deflected toward them. In addition, as the salt layer itself possesses strong plasticity, the propagating capacity of the hydraulic fractures is lower than that in the shale layers. Consequently, it can be inferred that fully developed bedding fractures, lithology interfaces, and other weak structures greatly restrict the growth of hydraulic fractures with regard to their direction and height, resulting in a small stimulation volume. Salt is generally considered to be soft with extremely low porosity; it is a low-permeability rock with self-healing capacity (De Las Cuevas, 1997; Liu et al., 2020b). In addition, drilling practice in nearby Wangchang area shows that high-pressure brine overflow occurs in part of the newly drilled wells. The reason for the overflow is an

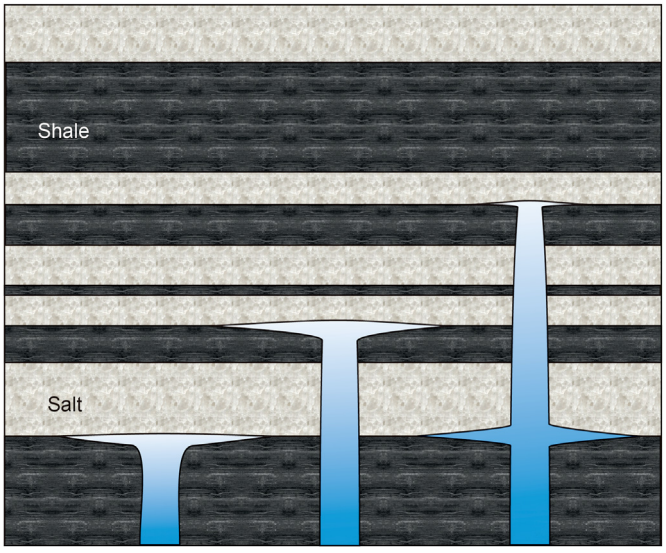

Fig. 20. Diagram of shielding and sealing effects of salt rock. Owing to the low strength of lithology interfaces and bedding places and the strong plasticity capacity of salt rock, it is difficult to propagate hydraulic fractures that intersect across salt layers.

increase in the pressure of the water from the nearby injecting wells, which occurs owing to these wells being sealed by the salt layers, thus reducing diffusion and inhibiting formation of more local high-pressure areas. Apparently, the tight salt layers have a sealing effect on the fracturing fluid. The salt layers may undergo greater plastic deformation after the fracturing fluid causes a local high pressure. The width of the artificial fracture increases significantly as the pressure inside the fracture increases, which is a valid explanation for the easy pumping of proppant during on-site operation. When pumping is stopped, the storage space for the fracturing fluid is reduced, owing to the salt rock creep; together with the sealing effect of the salt layer, the hydraulic pressure is difficult to diffusive. This is another good explanation for the fact that the pumping pressure does not drop after the injection stops. We infer that the above phenomena are the result of the weak strength of the lithology interfaces of the salt layer. In addition, the fracturing fluid is mainly stored in the space formed after the lithology interfaces are opened to ensure that the purpose of effective stimulation is not achieved. The weakness of the different types of interfaces is also one of the potential and important reasons for the sharp drop in the output of oil wells.

The generation and preservation mechanism of shale oil, and its migration law in pore and fracture structures are currently unclear yet. Current exploration and production technologies which are applied on shale oil formation cost more but the return is low. The inter-salt oil shale which as a special type of oil shale formation raises more problems and challenges during its exploitation, while with the inspiring exploration prospects, this kind of shale oil still should be brought to the forefront and more insightful investigation should be carried out.

When aiming at improving the effect of hydraulic fracturing in inter-salt oil shale formations, firstly, we think the integrated geophysics technique in reservoir is more and more important in the exploration and development of inter-salt oil shale, fine description of thin layers, including shale, salt, and dolomite, and its horizontal changes is the foundation of improving stimulation result. Secondly, the salt layers for inter-salt oil shale should be concerned carefully, because the dissolution and recrystallization of salt rock leads the significant change in seepage capability of fractures, and the salt is so soft that the propagation of hydraulic fractures is impeded. Thirdly, large-scale physical and numerical simulation should be carried out aimed the inter-salt oil shale formations considering the factors we mentioned in this paper, most important of all, the influence of salt rock on final hydraulic fracture network and seepage characteristics should be clarified clearly. In the end, we do think it is necessary to conduct those laboratory experiments and numerical simulations for hydraulic fracturing in inter-salt oil shale considering under a framework of multi-field coupling problems, as the thermal and chemical effects are also pretty obvious to the behaviors of salt rock and shale.

6. Conclusions

In view of the characteristics of inter-salt oil shale formations and the experimental results, the reasons for reducing the effectiveness of hydraulic fracturing were analyzed. Based on the results of this study, the following conclusions were reached:

Salt recrystallization does occur in fractures, dissolution and crystallization of saline minerals could reduce the fracture conductivity in fractures after hydraulic fracturing, and a greater temperature difference can accelerate this kind of decline. Rock samples from inter-salt layers exhibit low strength and plastic flow characteristics under low deviator stress conditions, which can lead to proppant embedment in fracture walls, hydraulic fractures close rapidly as it can not be supported effectively. The lithology interface

and bedding planes within the inter-salt oil shale formations are weakly cemented. It is difficult for the hydraulic fractures to cross through the interfaces, thus forming shielding and sealing effects, reducing the effective stimulated reservoir volume (ESRV). To maintain higher conductivity of hydraulic fractures, it is recommended to reduce or inhibit the ability of formation fluids and fracturing fluids to dissolve salt minerals. In addition, selecting appropriate proppant which the particle size and strength are suitable for the rock properties of inter-salt shale layers, is as well as important to improve fracture conductivity and effective connection in multiple shale layers.

Declaration of competing interest

The authors declare that they have no known competing financial interests or personal relationships that could have appeared to influence the work reported in this paper.

Acknowledgments

This research was supported by the National Natural Science Foundation of China (No. 52104046), and National Science and Technology Major Project of China (No. 2016ZX05060-004, 2017ZX05036-003). All authors would like to express their sincere gratitude to the editors and anonymous reviewers for their insightful comments, which have greatly improved the quality of this paper.

References

Barati, R., Liang, J.-T., 2014. A review of fracturing fluid systems used for hydraulic fracturing of oil and gas wells. J. Appl. Polym. Sci. 131 (16), 40735. https://doi.org/10.1002/app.40735.

Bayram, F., Bektasoglu, I., 2020. Determination of actual dissolution rates from some rock properties in construction of deep salt cavern for natural gas storage. Int. J. Rock Mech. Min. Sci. 126, 104183. https://doi.org/10.1016/j.ijrmms.2019.104183.

Boyer, C., Clark, B., Jochen, V., et al., 2011. Shale gas: a global resource. Oilfield Rev. 23, 28–39.

De Las Cuevas, C., 1997. Pore structure characterization in rock salt. Eng. Geol. 47 (1), 17–30. https://doi.org/10.1016/S0013-7952(96)00116-0.

Fan, X., Su, J.Z., Chang, X., et al., 2019. Brittleness evaluation of the inter-salt shale oil reservoir in Jianghan Basin in China. Mar. Petrol. Geol. 102, 109–115. https://doi.org/10.1016/j.marpetgeo.2018.12.013.

Fang, Z., 2002. Hydrocarbon exploration significant of intersalt sediments in qianjiang saline lake basin. Acta Sedimentol. Sin. 20 (4), 608–613 (in Chinese).

Fuenkajorn, K., Phueakphum, D., 2010. Effects of cyclic loading on mechanical properties of Maha Sarakham salt. Eng. Geol. 112 (1), 43–52. https://doi.org/10.1016/j.enggeo.2010.01.002.

Fuenkajorn, K., Sriapai, T., Samsri, P., 2012. Effects of loading rate on strength and deformability of Maha Sarakham salt. Eng. Geol. 135–136, 10–23. https://doi.org/10.1016/j.enggeo.2012.02.012.

Golding, S.D., Boreham, C.J., Esterle, J.S., 2013. Stable isotope geochemistry of coal bed and shale gas and related production waters: a review. Int. J. Coal Geol. 120, 24–40. https://doi.org/10.1016/j.coal.2013.09.001.

Guo, Y., Cai, Z., 2010. Experimental studies on mechanical properties of salt rock of Qianjiang Salt Mine. Min. Res. Dev. 30 (2), 23–27. https://doi.org/10.13827/j.cnki.kyyk.2010.02.021 (in Chinese).

Guo, Y., Yang, C., Mao, H., 2012. Mechanical properties of Jintan mine rock salt under complex stress paths. Int. J. Rock Mech. Min. Sci. 56, 54–61. https://doi.org/10.1016/j.ijrmms.2012.07.025.

Han, L., Huang, Y., Li, B., et al., 2016. Analysis of the effects of water-absorbing and recrystallization of glauberite on intra-salt reservoir. Offshore Oil 36 (1), 64–69 (in Chinese).

Han, Y., Ma, H., Yang, C., et al., 2021. The mechanical behavior of rock salt under different confining pressure unloading rates during compressed air energy storage (CAES). J. Petrol. Sci. Eng. 196, 107676. https://doi.org/10.1016/j.petrol.2020.107676.

Hou, Y., Wang, F., He, S., et al., 2017. Properties and shale oil potential of saline lacustrine shales in the Qianjiang Depression, Jianghan Basin, China. Mar. Petrol. Geol. 86, 1173–1190. https://doi.org/10.1016/j.marpetgeo.2017.07.008.

Hu, S., Zhao, W., Hou, L., et al., 2020. Development potential and technical strategy of continental shale oil in China. Petrol. Explor. Dev. 47 (4), 877–887. https://doi.org/10.1016/S1876-3804(20)60103-3.

Huang, H., 2018. Characteristics of hydrocarbon formation, migration, and accumulation in the jianghan saline lake basin. J. Southwest Petroleum Univ. (Science & Technology Edition) 40 (6), 69–76. https://doi.org/10.11885/j.issn.l6745-5086.2018.04.26.02 (in Chinese).

Jackson, R.B., Vengosh, A., Carey, J.W., et al., 2014. The environmental costs and benefits of fracking. Annu. Rev. Environ. Resour. 39 (1), 327–362. https://doi.org/10.1146/annurev-environ-031113-144051.

Jarvie, D.M., Hill, R.J., Ruble, T.E., et al., 2007. Unconventional shale-gas systems: the Mississippian Barnett Shale of north-central Texas as one model for thermogenic shale-gas assessment. AAPG (Am. Assoc. Pet. Geol.) Bull. 91 (4), 475–499. https://doi.org/10.1306/12190606068.

Jiang, Z., Zhang, W., Liang, C., et al., 2016. Basic characteristics and evaluation of shale oil reservoirs. Petroleum Research 1 (2), 149–163. https://doi.org/10.1016/S2096-2495(17)30039-X.

Jin, X., 2020. Application of CO_2 dry fracturing process in inter-salt shale oil in Jianghan Oilfield. J. Jianghan Petroleum Univ. Staff Workers 33 (2), 35–37 (in Chinese).

Khaledi, K., Mahmoudi, E., Datcheva, M., et al., 2016. Stability and serviceability of underground energy storage caverns in rock salt subjected to mechanical cyclic loading. Int. J. Rock Mech. Min. Sci. 86, 115–131. https://doi.org/10.1016/j.ijrmms.2016.04.010.

Li, H., Yang, C., Ma, H., et al., 2020. A 3D grain-based creep model (3D-GBCM) for simulating long-term mechanical characteristic of rock salt. J. Petrol. Sci. Eng. 185, 106672. https://doi.org/10.1016/j.petrol.2019.106672.

Li, H., Yang, J., Han, Y., et al., 2019. Weibull grain-based model (W-GBM) for simulating heterogeneous mechanical characteristics of salt rock. Eng. Anal. Bound. Elem. 108, 227–243. https://doi.org/10.1016/j.enganabound.2019.09.001.

Li, M., Chen, Z., Cao, T., et al., 2018. Expelled oils and their impacts on rock-eval data interpretation, Eocene Qianjiang Formation in Jianghan Basin, China. Int. J. Coal Geol. 191, 37–48. https://doi.org/10.1016/j.coal.2018.03.001.

Li, X.-E., Yin, H.-Y., Zhang, R.-S., et al., 2019. A salt-induced viscosifying smart polymer for fracturing inter-salt shale oil reservoirs. Petrol. Sci. 16 (4), 816–829. https://doi.org/10.1007/s12182-019-0329-3.

Liang, W., Zhang, C., Gao, H., et al., 2012. Experiments on mechanical properties of salt rocks under cyclic loading. J. Rock Mech. Geotech. Eng. 4 (1), 54–61. https://doi.org/10.3724/SP.J.1235.2012.00054.

Liu, W., Zhang, X., Fan, J., et al., 2020a. Study on the mechanical properties of man-made salt rock samples with impurities. J. Nat. Gas Sci. Eng. 84, 103683. https://doi.org/10.1016/j.jngse.2020.103683.

Liu, W., Zhang, Z., Fan, J., et al., 2020b. Research on gas leakage and collapse in the cavern roof of underground natural gas storage in thinly bedded salt rocks. J. Energy Storage 31, 101669. https://doi.org/10.1016/j.est.2020.101669.

Ma, C., Li, L., Xiao, J., et al., 2015. Analysis of formation water and regularity of salt of the salt interstratification in Wangchang oilfield. Sci. Technol. Eng. 15 (35), 165–169.

Ma, L., Liu, X., Wang, M., et al., 2013. Experimental investigation of the mechanical properties of rock salt under triaxial cyclic loading. Int. J. Rock Mech. Min. Sci. 62, 34–41. https://doi.org/10.1016/j.ijrmms.2013.04.003.

Ma, L., Xu, H., Tong, Q., et al., 2014. Post-yield plastic frictional parameters of a rock salt using the concept of mobilized strength. Eng. Geol. 177, 25–31. https://doi.org/10.1016/j.enggeo.2014.05.003.

Mansouri, H., Ajalloeian, R., 2018. Mechanical behavior of salt rock under uniaxial compression and creep tests. Int. J. Rock Mech. Min. Sci. 110, 19–27. https://doi.org/10.1016/j.ijrmms.2018.07.006.

Melikoglu, M., 2014. Shale gas: analysis of its role in the global energy market. Renew. Sustain. Energy Rev. 37, 460–468. https://doi.org/10.1016/j.rser.2014.05.002.

Ministry of Natural Resources of PRC, 2020. In: Ling, Y. (Ed.), China Mineral Resources 2020. Beijing: Ministry of Natural Resources of PRC.

Philp, R.P., Fan, Z., 1987. Geochemical investigation of oils and source rocks from Qianjiang depression of Jianghan basin, a terrigenous saline basin, China. Org. Geochem. 11 (6), 549–562. https://doi.org/10.1016/0146-6380(87)90009-X.

Singh, A., Kumar, C., Gopi Kannan, L., et al., 2018a. Engineering properties of rock salt and simplified closed-form deformation solution for circular opening in rock salt under the true triaxial stress state. Eng. Geol. 243, 218–230. https://doi.org/10.1016/j.enggeo.2018.07.008.

Singh, A., Kumar, C., Kannan, L.G., et al., 2018b. Estimation of creep parameters of rock salt from uniaxial compression tests. Int. J. Rock Mech. Min. Sci. 107, 243–248. https://doi.org/10.1016/j.ijrmms.2018.04.037.

Slatt, R.M., 2011. Important geological properties of unconventional resource shales. Cent. Eur. J. Geosci. 3 (4), 435–448. https://doi.org/10.2478/s13533-011-0042-2.

Sun, Z., Wang, F., Han, Y., et al., 2020. Multi-scale characterization of the spatial distribution of movable hydrocarbon in intersalt shale of Qianjiang Formation, Qianjiang Sag, Jianghan Basin. Petroleum Geology & Experiment 42 (4), 586–595. https://doi.org/10.11781/sysydz202004586 (in Chinese).

Taheri, S.R., Pak, A., Shad, S., et al., 2020. Investigation of rock salt layer creep and its effects on casing collapse. Int. J. Min. Sci. Technol. 30 (3), 357–365. https://doi.org/10.1016/j.ijmst.2020.02.001.

Vengosh, A., Warner, N., Jackson, R., et al., 2013. The effects of shale gas exploration and hydraulic fracturing on the quality of water resources in the United States. Procedia Earth Planetary Sci. 7, 863–866. https://doi.org/10.1016/j.proeps.2013.03.213.

Wang, G., Guo, K., Christianson, M., et al., 2011. Deformation characteristics of rock salt with mudstone interbeds surrounding gas and oil storage cavern. Int. J. Rock Mech. Min. Sci. 48 (6), 871–877. https://doi.org/10.1016/j.ijrmms.2011.06.012.

Wang, J., Zhang, Q., Song, Z., et al., 2021. Experimental study on creep properties of

salt rock under long-period cyclic loading. Int. J. Fatig. 143, 106009. https://doi.org/10.1016/j.ijfatigue.2020.106009.
Wang, M., Guo, Z., Jiao, C., et al., 2019. Exploration progress and geochemical features of lacustrine shale oils in China. J. Petrol. Sci. Eng. 178, 975–986. https://doi.org/10.1016/j.petrol.2019.04.029.
Wang, R., 2015. Adaptability analysis of measures for inter-salt argillaceous dolomite reservoir in Qianjiang Sag. Technology Outlook 25 (14), 170 (in Chinese).
Wang, Z., Tang, Y., Wang, Y., et al., 2020. Kinetics of shale oil generation from kerogen in saline basin and its exploration significance: an example from the Eocene Qianjiang Formation, Jianghan Basin, China. J. Anal. Appl. Pyrol. 150, 104885. https://doi.org/10.1016/j.jaap.2020.104885.
Wanyan, Q., Xiao, Y., Tang, N., 2019. Numerical simulation and experimental study on dissolving characteristics of layered salt rocks. Chin. J. Chem. Eng. 27 (5), 1030–1036. https://doi.org/10.1016/j.cjche.2019.01.004.
Wu, S., Tang, X., Du, X., et al., 2013. Geologic characteristics of continental shale oil in the qianjiang depression, Jianghan salt lake basin. J. East China Inst. Technol. 36 (3), 282–286. https://doi.org/10.3969/j.issn.1674-3504.2013.03.006 (in Chinese).
Yang, C., Daemen, J.J.K., Yin, J.-H., 1999. Experimental investigation of creep behavior of salt rock. Int. J. Rock Mech. Min. Sci. 36 (2), 233–242. https://doi.org/10.1016/S0148-9062(98)00187-9.
Yang, F., Ning, Z., Liu, H., 2014. Fractal characteristics of shales from a shale gas reservoir in the Sichuan Basin, China. Fuel 115, 378–384. https://doi.org/10.1016/j.fuel.2013.07.040.
Yang, Z., Li, R., Li, H., et al., 2020. Experimental evaluation of the salt dissolution in intersalt shale oil reservoirs and its influence on porous flow. Petrol. Explor. Dev. 47 (4), 803–809. https://doi.org/10.1016/S1876-3804(20)60095-7.
Yin, H., Yang, C., Ma, H., et al., 2019. Study on damage and repair mechanical characteristics of rock salt under uniaxial compression. Rock Mech. Rock Eng. 52 (3), 659–671. https://doi.org/10.1007/s00603-018-1604-0.
Zhang, H., Wang, Z., Zheng, Y., et al., 2012. Study on tri-axial creep experiment and constitutive relation of different rock salt. Saf. Sci. 50 (4), 801–805. https://doi.org/10.1016/j.ssci.2011.08.030.
Zhang, Y., Yang, Y., Qi, Z., et al., 2003. Sedimentary characteristics and environments of the salt-bearing series of qianjiang formation of the paleogene in qianjiang sag of jianghan basin. J. Palaeogeogr. 5 (1), 29–35 (in Chinese).
Zhi, Y., Caineng, Z., Songtao, W., et al., 2019. Formation, distribution and resource potential of the "sweet areas (sections)" of continental shale oil in China. Mar. Petrol. Geol. 102, 48–60. https://doi.org/10.1016/j.marpetgeo.2018.11.049.
Zou, C., Pan, S., Jing, Z., et al., 2020. Shale oil and gas revolution and its impact. Acta Pet. Sin. 41 (1), 1–12. https://doi.org/10.7623/syxb202001001 (in Chinese).